Electroelastic unpinning of rotating vortices in biological excitable media

C. Cherubini,[1,2] S. Filippi,[1,2] and A. Gizzi[1,3]

[1]*Nonlinear Physics and Mathematical Modeling Lab, University Campus Bio-Medico, I-00128 Rome, Italy*

[2]*International Center for Relativistic Astrophysics, University of Rome "La Sapienza," I-00185 Rome, Italy*

[3]*Alberto Sordi Foundation, Research Institute on Aging, I-00128 Rome, Italy*

(Received 3 August 2011; revised manuscript received 22 February 2012; published 28 March 2012)

Spiral waves in excitable biological media are associated with pathological situations. In the heart an action potential vortex pinned by an obstacle has to be removed through defibrillation protocols fine-tuned theoretically by using electrophysiological nonlinear mathematical models. Cardiac tissue, however, is an electroelastic medium whose electrical properties are strongly affected by large deformations. In this paper we specifically investigate the electroelastic pinning-unpinning mechanism in order to include cardiac contraction in the preexisting theoretically modeled defibrillation scenarios. Based on a two-dimensional minimal electromechanical model, we show numerically the existence of an unpinning band characterized by the size of the obstacle, the pacing site, and the frequency. Similar numerical simulations, performed in the absence of elastic coupling, show small differences in comparison with the electroelastic studies, suggesting for this specific scenario of pinning-unpinning dynamics a nonprominent role of elasticity.

DOI: 10.1103/PhysRevE.85.031915 PACS number(s): 87.19.Hh, 05.45.−a, 87.10.Pq, 46.25.Hf

I. INTRODUCTION

A wide range of spiral wave behaviors can be recognized in many different natural systems [1–7]. Such a phenomenon has relevance in particular in heart dynamics in association with dangerous and even lethal pathologies [8–10]. Spiral control is mandatory then, but while such an action can easily be achieved in homogeneous active media (cell cultures typically [11–13]), it becomes an extremely complicated problem in heterogeneous systems. The so-called pinning regions (for example, scar in heart tissue or large vessels) in fact represent spatial obstacles, characterized by altered electrophysiological properties, which tend to attach a propagating spiral wave in a persistent manner.

A pinned spiral in the heart muscle can be removed by a weak electric pulse delivered at the boundary of the obstacle [14–16]. Advanced techniques have been proposed however, in order to use wave trains for sudden termination of pinned systems [5,17–19]. The low-energy defibrillation procedures proposed to remove spiral reentries both *in vitro* and *in vivo* appear to be even more complicated [20]. Many of these studies adopt mathematical models fine-tuned with experiments in order to give predictions for applications. Most of these analyses, however, neglect mechanical deformations induced by electrical activity. The main reason for this is that continuum mechanics is a complicated nonlinear physical theory and there is little experimental data in comparison with the cases (nondeformable) in which contraction is blocked through calcium or gating blockers [21,22]. While in excitable media such as nerves elastic deformations due to voltage passage are very small [23,24], cardiac tissue undergoes very large deformations (a myocite can change its elongation up to 20% of its rest length [25–30]), requiring finite elasticity theory.

The heart is an electrically driven mechanical pump. Studies on isolated tissues and whole hearts have shown that mechanical stimuli can affect both cardiac electrical excitation and wave spread due to the presence of mechanosensitive ion channels. Such a behavior has been specifically termed mechanoelectric feedback [31–33] and its effects range from physiological heart rate modulation to the mechanical induction of heart rhythm disturbances or to their mechanical termination (see Refs. [34,35] and references therein). The necessity to include and understand the effects of mechanical deformations on the delicate problem of spiral wave pinning and unpinning thus appears to be mandatory.

This point is discussed theoretically in this paper using a minimal mechanical model that has been fine-tuned to qualitatively fit electrophysiological experiments. The main reason for this choice is the exiguity of mechanoelectrical experimental studies in comparison with the very large amount of electrophysiological ones. The main outcome of the present analysis in particular consists in exploring the role of elasticity during electrical defibrillation of a pathologic portion of cardiac tissue. An important point addressed here, relevant for both experimental and clinical arrhythmia studies [35,36], is the theoretical existence of an unpinning band, i.e., the full range of defibrillation pacing periods that enable the detachment (unpinning) of an action potential wave (pinned spiral) rotating in a persistent manner around a circular heterogeneity of the medium (obstacle). This mathematical tool can be defined in both the presence and absence of elastic coupling. In both of these cases this band has been quantified in its variability with respect to the size of the obstacle, the pacing period, and position of external stimulation current on the lines of the purely electrical (i.e., rigid) analysis reported in Ref. [17]. The main outcome of the analyses performed here is the fact that the presence of elastic coupling does not seem to change the pinning-unpinning dynamics dramatically in comparison with nonelastic situations. This is somewhat an unexpected result due to the strong nonlinear nature of all the physical equations involved, although electroelastic coupling may in any case still play an important role in other situations such as free spiral dynamics in large domains and generation of turbulent cardiac regimes.

The paper is organized as follows. After the Introduction, in Sec. II we describe the conventions adopted to formulate the model, reporting the continuum mechanics balance equations with associated constitutive prescriptions for both the passive and active deformation schemes [37]. We then

present the three-variable phenomenological Fenton-Karma model of cardiac action potential [38], here coupled with an additional basic nondiffusive calcium dynamics and finite elasticity equations along the lines of Refs. [39,40]. In Sec. III we discuss a set of numerical simulations reporting the successful electrical defibrillation events on a two-dimensional electroelastic medium, in which an action potential spiral wave is pinned by a circular nonexcitable portion of tissue located at the center of the domain. In Sec. IV we analyze the physical implications of our study and the possible future extensions of our work.

II. MODEL

Mechanoelectric feedback can be modeled by assuming that when cardiac muscle fibers are stimulated, these generate contractile forces that, at the macroscopic scale of the tissue, are described by an active stress tensor constitutively related to the tissue's electrophysiological activity. The overall stress in the tissue is then recovered by adding a passive one to the active stress, depending on the mechanical properties of the myocardium [41–44]. While the distribution of muscle fibers influences the active response of the tissue, the spatial variation in collagen distribution is related to the material constitutive parameters and determines the nonlinear anisotropic passive response of the tissue. Here we adopt the point of view presented in Ref. [37], which introduces the notion of active deformation as alternative to that of active stress motivated by the wide range of constitutive theories based on this approach [45]. We assume that, at the macroscopic scale, the activation of a cardiac muscle fiber is described by the change in its rest length; then the stress state in the activated tissue is due to the difference between its actual configuration and its rest state. The active deformation is in turn related to the electrophysiological activity of the tissue. As suggested by many experiments, calcium concentration is the main factor driving the variation in the rest length of muscles. In this study the electromechanical model of myocardium proposed in Ref. [39] has been generalized by adopting the three-variable electrophysiological model of Fenton and Karma [38]. The high degree of deformability of the medium makes it mandatory to set the diffusion process in a moving deformable domain, thereby producing a direct influence of the deformation on the electrical activity. We now give the various ingredients of the model just described.

(a) Conventions. The model equations are defined using a general curvilinear coordinate system relating a reference (material or undeformed) domain with a current (spatial or deformed) one. From standard continuum mechanics we denote X_I $(I = 1,2,3)$ as the coordinates in the reference domain B with boundary ∂B and x_i $(i = 1,2,3)$ as the coordinates in the current domain B_0 with boundary ∂B_0. An uppercase subscript refers to the reference configuration while lowercase refers to the current one. The relation between the two coordinate systems is geometrically defined by the deformation gradient tensor $F_{iJ} = (\partial x_i/\partial X_J)$, from which $J = \det(F_{iJ}) = (\rho_o/\rho)$ can be defined, representing the volume change (density ratio) during motion [46].

We assume a multiplicative decomposition [32] of the deformation gradient tensor into a passive and an active part $F_{iJ} = F^e_{iK} F^a_{KJ}$, leading to the implicit definition of the elastic deformation tensor $F^e_{iK} = F_{iJ}(F^a_{JK})^{-1}$. Such an assumption splits the elastic and active responses on F^e_{iJ} and F^a_{IJ}, respectively. We assume the right Cauchy-Green strain tensor $C^e_{IJ} = F^e_{kI} F^e_{kJ}$ as the elastic deformation measure of the body. In our modeling the medium is treated as incompressible in only the elastic (passive) behavior, with the corresponding incompressibility kinematic constraint given by $\det(C^e_{IJ}) = 1$.

Taking the strain energy function $\psi = \psi(C^e_{IJ})$ and applying the standard variational method [47] with respect to the elastic measure of deformation C^e_{IJ}, we define the second Piola-Kirchhoff stress tensor S_{IJ} as

$$S_{IJ} = 2\frac{\partial \psi}{\partial C^e_{IJ}} - p{C^e_{IJ}}^{-1}. \tag{1}$$

In this relation p represents the hydrostatic pressure (a Lagrange multiplier) necessary to satisfy the incompressibility constraint. In order to adopt the balance equation we introduce the first Piola-Kirchoof stress tensor $P_{iJ} = F_{iK} S_{KJ}$.

(b) Continuum mechanics balance equations. Imposing the conservation of linear momentum in the reference configuration and neglecting inertial terms, we get Eq. (2) in the reference domain B and Eq. (3) on its boundary ∂B:

$$0 = \frac{\partial}{\partial X_I} P_{IJ} \quad \text{in } B, \tag{2}$$

$$t_I = N_J P_{IJ} \quad \text{on } \partial B. \tag{3}$$

Equation (3) introduces the normal N_J in the reference domain, which can be derived from its current (deformed) representation using Nanson's formula relating the surface area elements between the two configurations ($n_i ds = J F^{-1}_{Ii} N_I dS$ [47]).

(c) Constitutive prescriptions. The nature of cardiac tissue is extremely complex in the passive mechanical response [48]. Here we focus mainly on the coupling between mechanical deformation and electrophysiological aspects, treating the myocardium as a homogeneous, elastic, isotropic, and incompressible tissue. Adopting a neo-Hookean incompressible material representation (with all the mechanical quantities normalized by the elastic modulus α_1; see [40] for details), the elastic strain energy ψ depends only on the first invariant of the right Cauchy-Green elastic strain tensor $I_1 = \mathrm{tr}({C_{IJ}}^e)$, so we can write

$$\psi(I_1) = \frac{\alpha_1}{2}(I_1 - 3). \tag{4}$$

This is a classical choice because C^e_{IJ} collects the complete information on the stretches experienced in any of the three orthogonal directions.

In our minimal model we assume a planar, isotropic muscle fiber distribution defined by the unit vector h_I. At the macroscopic scale the activation of the muscle fibers is prescribed by the active deformation field expressed by

$$F^a_{IJ} = \gamma_0(c)(\delta_{IJ} - h_I h_J). \tag{5}$$

The active stretch $\gamma_0(c)$ measures the amount of active contraction of any fiber and accounts for the relation between calcium c dynamics and deformation.

The constitutive characterization of the boundaries aims to mimic the tissue surrounding the patch, i.e.,

$$t_I = -k^b \delta_{IJ} U_J. \tag{6}$$

We assume that the reference traction density t_I depends linearly on the boundary displacement U_J through an isotropic stiffness tensor $K_{IJ} = k^b \delta_{IJ}$, where k^b is a dimensionless parameter mimicking the stiffness of the surrounding tissue.

(d) Electrophysiological equations. The adopted nondimensional model of cardiac action potential propagation [38] in the reference configuration assumes the form

$$\frac{\partial u}{\partial t} = \frac{1}{J}\frac{\partial}{\partial X_J}\left(J D_{IJ}\frac{\partial u}{\partial X_I}\right) + I_{\text{ion}}, \tag{7}$$

$$\frac{\partial v}{\partial t} = \theta_c\left(\frac{1-v}{\tau_v^-}\right) - (1-\theta_c)\frac{v}{\tau_v^+}, \tag{8}$$

$$\frac{\partial w}{\partial t} = \theta_c\left(\frac{1-w}{\tau_w^-}\right) - (1-\theta_c)\frac{w}{\tau_w^+}. \tag{9}$$

It consists of three variables: the membrane potential u plus a fast and a slow transmembrane ionic gate, v and w, respectively; $\theta_c = \theta_c(u - u_c)$ is the standard Heaviside function and D_{IJ} is the diffusion tensor expressed in the reference coordinates and mapped via F_{iJ} (pullback) from its current representation D_{ij} following the geometric transformation $D_{IJ} = F_{jJ}^{-1} D_{ij} F_{Ii}^{-1}$. Assuming tissue isotropy, we have $D_{ij} = d_o I_{ij}$, with I_{ij} the unit tensor and d_o the constant intensity in the three orthogonal directions; $I_{\text{ion}} = I_{\text{fi}} + I_{\text{so}} + I_{\text{si}}$ is the total transmembrane density current, which is the sum of a fast inward inactivation current I_{fi}, a slow time-independent rectifying outward current I_{so}, and a slow inward inactivation current I_{si}. Their expressions are given by

$$I_{\text{fi}} = -\frac{v}{\tau_d}\theta_c(1-u)(u-u_c), \tag{10}$$

$$I_{\text{so}} = \frac{u}{\tau_o}(1-\theta_c) + \frac{1}{\tau_r}\theta_c, \tag{11}$$

$$I_{\text{si}} = -\frac{w}{2\tau_{\text{si}}}\left\{1 + \tanh\left[k\left(u - u_c^{\text{si}}\right)\right]\right\}. \tag{12}$$

The time constant governing the reactivation of the fast inward current is given by

$$\tau_v^-(u) = \theta_v \tau_{v1}^- + (1-\theta_v)\tau_{v2}^- \tag{13}$$

and is defined over two voltage ranges ($u_v < u < u_c$ and $u < u_v$) ruled by the Heaviside function θ_v.

We have adopted a parametric setup fitted for a modified version of the Beeler-Reuter model, giving a circular meandering for a free spiral on a homogeneous and isotropic domain. Equations (7)–(9) describe a normalized dimensionless membrane potential, ranging from 0 to 1, while the mapping $u = (V_m - V_0)/(V_{\text{fi}} - V_0)$ recovers the physical quantity measured in millivolts (see Ref. [38] for details). Here V_m stands for transmembrane potential, V_0 is the resting membrane potential, and V_{fi} is the Nernst potential of the fast inward current (model parameters are reported in Table I).

(e) Electro-mechanical coupling. Here we assume the role of free Ca^{2+} ions in the activation mechanism of the contraction process as well as the sensitivity of cardiac tissue to Ca^{2+} modeled by

TABLE I. Adopted model parameters for the modified Beeler-Reuter electric setup [38] and finite elasticity [39] (M stands for mol/l).

$u_c = 0.13$	$u_v = 0.055$
$u_c^{si} = 0.85$	$\bar{g}_{\text{fi}} = 4$
$\tau_r = 50$ ms	$\tau_{\text{si}} = 45$ ms
$\tau_0 = 8.3$ ms	$\tau_v^+ = 3.33$ ms
$\tau_0 = 8.3$ ms	$\tau_{v1}^- = 1000$ ms
$\tau_{v2}^- = 19.6$ ms	$\tau_w^+ = 667$ ms
$\tau_w^- = 11$ ms	$k = 8$
$d_o = 10^{-3}$ cm^2/ms	$V_0 = -85$ mV
$V_{fi} = 15$ mV	$V_{\text{Ca}} = 300$ mV
$c_0 = 3.2 \times 10^{-7} M$	$c^* = 10^{-7} M$
$\gamma_0(c^*) = 1$	$\gamma_0^{\max} = 0.8$
$\beta = 6$	$q_{\text{Ca}} = 2 \times 10^{-6}$
$k_{\text{Ca}} = 3256\ ms^{-1}$	$k^b = 0.1$

$$\frac{\partial c}{\partial t} = q_{\text{Ca}}(u + V_{\text{Ca}}) - k_{\text{Ca}} c, \tag{14}$$

where c is the scalar field describing calcium concentration. A linear coupling is assumed between membrane voltage u and calcium concentration c. The proposed mass balance equation is a nondiffusive version of more general reaction-diffusion systems needed for a realistic handling of calcium dynamics [49,50]. This minimal choice has been motivated by the main aim of this paper, which is to explore the most basic nature of the anatomic reentry defibrillation scheme on a deformable isotropic excitable medium.

The remaining expressions for electromechanical coupling are

$$\gamma_0(c) = \frac{\lambda_{\text{Ca}}}{1 + f_{\text{Ca}}(c)(\lambda_{\text{Ca}} - 1)}\gamma_0^{\max}, \tag{15}$$

$$\lambda_{\text{Ca}} = \frac{f_{\text{Ca}}(c^*) - 1}{f_{\text{Ca}}(c^*) - \gamma_0^{\max}}, \tag{16}$$

$$f_{\text{Ca}}(c) = \frac{1}{2} + \frac{1}{\pi}\arctan\left(\beta_c \ln\frac{c}{c_0}\right), \tag{17}$$

along the lines of Ref. [39]. Here $\gamma_0(c)$ rules the active deformation scheme entering the definition of F_{IJ}^a [Eq. (5)], while λ_{Ca} and f_{Ca} are *ad hoc* functions necessary to induce the active contraction following calcium variations.

III. RESULTS

The electromechanical model (7)–(17) has been integrated numerically through a direct PARDISO finite-element method scheme [51,52] with a nested dissection preordering algorithm on the COMSOL MULTIPHYSICS 3.5*a* software [53]. Different square areas (side lengths $L = 5,6,7$ cm) have been adopted as the simulation domain. Each simulation has been run for $T = 3000$ ms of model time. An adaptive time-stepping procedure with a tolerance of 10^{-5} has been adopted, limiting the maximum time step to 0.2 ms. The complete set of simulations consisted of more than 500 distinct runs for a computational time of several months on a multiprocessor machine.

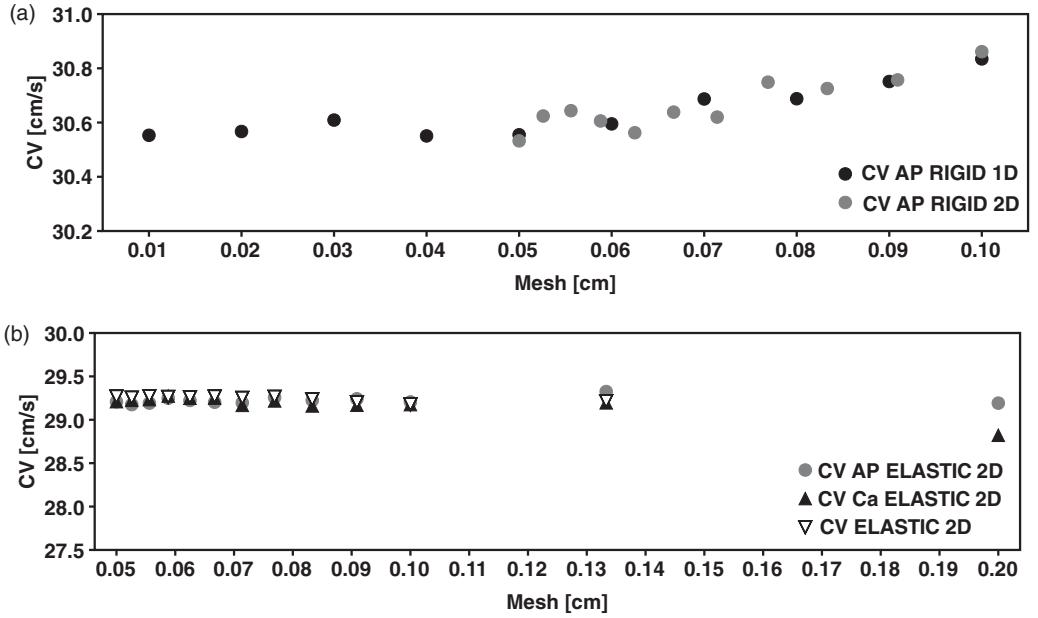

FIG. 1. Conduction velocity (CV) versus mesh size restitution graphs. Action potential (AP), elastic, and calcium (Ca) (kinematic) waves are compared to set the right mesh size for numerical solution purposes. The plane-wave traveling front timing has been taken at the 35% of its upstroke at two consecutive mesh positions nodes in order to evaluate the resulting velocity (several mesh nodes sequences have been tested). (a) Purely electric AP conduction velocities are compared between one-dimensional (1D) (black) and 2D (gray) simulation domains; (b) AP (gray circles), Ca (black triangles), and EL (gray triangles) conduction velocities are compared for a 2D simulation domain where the electric mesh has been kept fixed at $dx = 0.5$ cm. Estimated velocities for mesh sizes lower than $dx = 0.1$ cm present similar values.

The numerics has been fine-tuned upon several different simulation protocols. The mesh size has been explored for both the purely electric or rigid and coupled electromechanical models, as reported in Fig. 1. The procedure consisted in evaluating the conduction velocity of action potential (AP) and elastic waves, as well as calcium (kinematic waves [54]), for different regular square meshes adopting Lagrange quadratic elements until we reached stable flat curves. The electric problem results mesh independently for mesh sizes $dx \leqslant 0.07$ cm in both one and two dimensions [Fig. 1(a)]. In order to evaluate the minimal electromechanical mesh size we solved the two-dimensional coupled problem adopting different grids for the AP and Ca elastic waves, respectively. For a fixed AP grid $dx = 0.05$ cm, we obtained flat Ca elastic wave conduction velocities for a mesh size $dx \leqslant 0.1$ cm. On this basis, we finally chose a unique mesh size $dx = 0.067$ cm for the complete coupled model; we further subdivided each square mesh element into triangles in order to increase the accuracy and convergence of the numerical solution. The main results of this article (i.e., the unpinning band) are thus insensitive to the mesh size.

Zero-flux boundary conditions on the current (deformed) border have been imposed for AP variables while the mechanical boundaries, as anticipated, have been modeled as spring dynamics (analogous to rubber sample experiments [55]). Tissue heterogeneity has been introduced in the center of the domain and modeled as a nonexcitable circular obstacle with altered mechanical properties. Therein no action potential can generate or propagate, i.e., no diffusion $d_0 = 0$ cm^2/ms static ion dynamics, and the patch is considered stiffer than the surrounding tissue, i.e., the Young modulus has been lowered to 10%. The obstacle radius is in the range 0.35 cm $\leqslant R_{\mathrm{ob}} \leqslant$ 1.4 cm, in which discrete values have been selected with a finite step of 1.0 cm. An intermediate radius $R_{\mathrm{ob}} = 0.75$ cm has been tested too in order to verify the resulting trend. The lower limit $R_{\mathrm{ob}} = 0.35$ cm is forced by the choice of electric parameters whereby spiral pinning is no longer possible for smaller obstacles. The upper limit $R_{\mathrm{ob}} = 1.4$ cm is forced by both the domain size (which has to fit the anatomy of a large mammal ventricle such as a pig, dog, or human) and the unpinning trend band (discussed in the following), which tends to shrink, meaning that a purely electrical defibrillation is no longer possible at any stimulation period. This result is in accordance with the nondeformable numerical simulations reported in Ref. [17].

Tissue stimulation has been electrically induced as a circular electrode centered on the upper-left corner of the domain and characterized by a radius $R_p = 0.4$ cm. The pulse duration has been fixed at $\tau = 2$ ms with a dimensionless amplitude of 1.5. The stimulation protocol consisted in delivering regular sequences of squared waves at constant periods and for 3000 ms of simulation time or until spiral unpinning occurs. For each tested obstacle radius and starting from the same initial conditions, the stimulation period has been varied in the range 90–120 ms with a finite time step of 2 ms, for a total amount of 15 simulations.

Our numerical results show that the electroelastic medium is characterized by small differences with respect to the rigid one. Figure 2(a) shows the spiraling period around the circular obstacle comparing the rigid with the elastic cases. The two periods are separated following an almost linear interpolated trend and reaching the largest difference of 34 ms for the largest

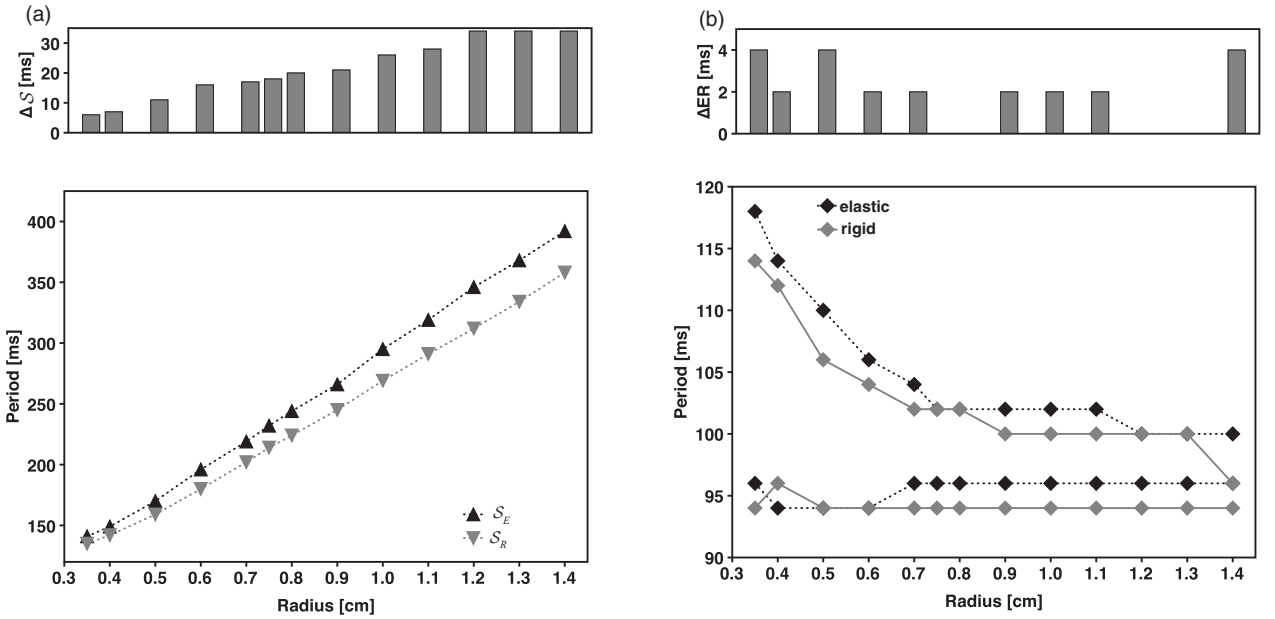

FIG. 2. Overall results from the explored simulations set. (a) Spiral rotational period compared for purely electric or rigid (gray) and electromechanic or elastic (black) simulations versus obstacle radius. The superimposed histogram shows the difference between the two cases highlighting a divergence trend that reaches its maximum value of 34 ms for the higher radii analyzed. (b) Comparison of the unpinning bands (upper and lower defibrillation limits) for the purely electric (gray) and the electromechanic (black) cases. The vertical axis reports the lowest and highest successful stimulation periods (in milliseconds), i.e., the ones for which the unpinning has been reached, having explored the range of periods 90–120 ms with a finite time step of 2 ms. The horizontal axis reports the discrete simulated obstacle radii ranging between 3.5 and 1.4 cm with a spatial step of 1 cm. The intermedium case $R_{ob} = 0.75$ cm has been tested in order to verify the resulting trend. The superimposed histogram shows the absolute difference of the band ranges between the two models. Both trends are highly nonlinear and reach their minimum range of frequencies for the larger obstacle radii analyzed.

obstacle radius we analyzed, $R = 1.4$ cm. The superimposed histogram enhances this difference plotting $\Delta\mathcal{S} = \mathcal{S}_E - \mathcal{S}_R$, where $\mathcal{S}_E$ and $\mathcal{S}_R$ are the spiral rotational periods in the elastic and rigid cases, respectively.

Despite such an elastic separation effect, the resulting unpinning trends are very similar in both shape and period as reported in Fig. 2(b), even if they present a strong nonlinearity, and become almost flat for larger obstacles. The graph indicates on the vertical axis the lowest and highest stimulation periods, respectively, which are able to detach the rotating spiral away from the obstacle. The horizontal axis shows the discrete radius values tested. The superimposed curves (black for elastic, gray for rigid) reveal that the elastic case can be defibrillated for stimulation periods greater than (or at least equal to) the rigid one. The matching of the two lines can be motivated by the changes of rate adopted to increase the stimulation period, i.e., 2 ms (which gives the graph resolution on the y axis). The overimposed histogram shows the difference between the two modeling bands as $\Delta ER = (T^{\text{elastic}}_{\text{max}} - T^{\text{elastic}}_{\text{min}}) - (T^{\text{rigid}}_{\text{max}} - T^{\text{rigid}}_{\text{min}})$, where the T are

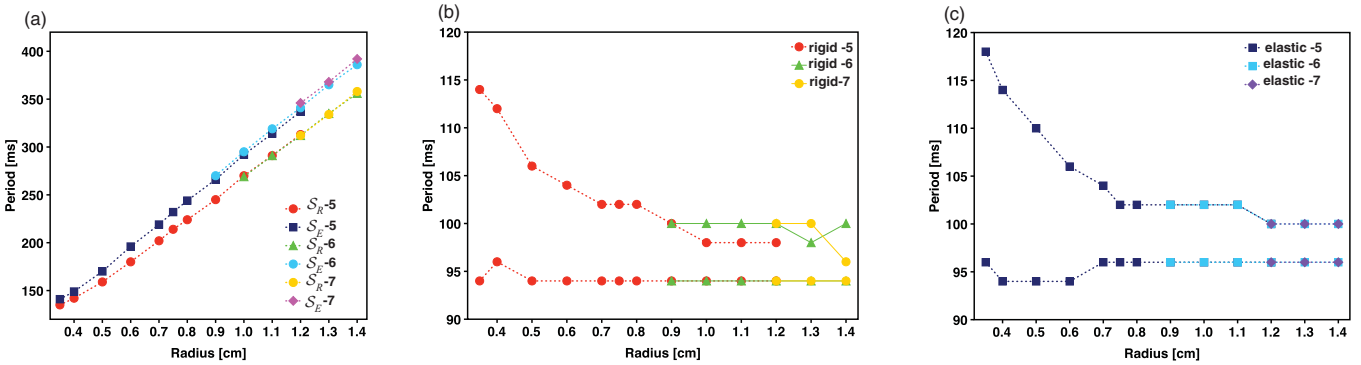

FIG. 3. (Color online) Comparison of the spiral rotation and successful defibrillation periods for three different domain sizes $L = 5,6,7$ cm for both rigid and elastic modeling versus obstacle radius. The spiral rotational periods (a) seem to be unaffected by changing the domain size, following the same behavior as reported in the previous case. In the purely electric case (b) the boundary effects induce a reduction of the unpinning band when the ratio $R_{ob}/L \geqslant 0.2$, while the electroelastic model (c) shows a better robustness to this effect.

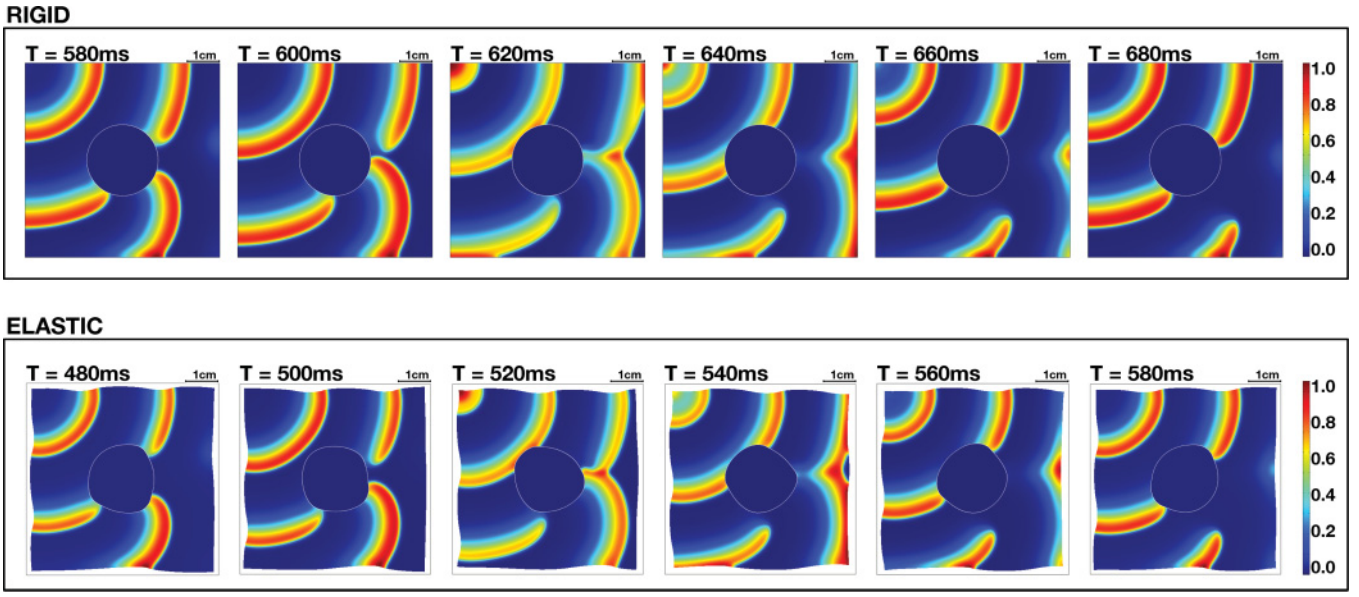

FIG. 4. (Color online) Sequences of defibrillation scenarios with no elasticity (top row, rigid) and contraction activated (bottom row, elastic). Both sequences refer to a domain size $L = 6$ cm, an obstacle radius $R_{ob} = 1.2$ cm, and a stimulation period $T = 100$ ms. The timing reported in the panels shows a shifting in the unpinning event between the two cases. The color map referred to is the normalized action potential of the Fenton-Karma model [38].

the maximum and minimum successful stimulation unpinning periods. This result reveals that major differences can be found for the smaller as well as for the higher radii analyzed. In these extreme cases the explanation can be found respectively in weak attaching of the AP waves for small obstacles and in boundary effects for larger ones. Our results seem to confirm the work presented in Ref. [17], where a maximum obstacle size for unpinning is reached depending on the spiral meandering radius R_s. In fact, as reported in Fig. 2(b), we find a minimum band amplitude at $R = 1.4$ cm. Our choice of parameters gives a free rigid spiral meandering with rotation period $T_s^R = 147$ ms and radius $R_s^R \sim 0.35$ cm, while for the elastic one $T_s^E = 176$ ms and $R_s^E \sim 0.4$ cm. The small increase of the electroelastic free spiral meandering is consistent with the results shown and underlines the importance of the nonlinear mechanical feedback on the overall dynamics.

We also tested our results for different domain sizes $L = 5,6,7$ cm in order to minimize the boundary effects and to make the unpinning band discussion independent of the pacing site. In Fig. 3 we show the comparison between the unpinning and the spiraling rotation periods for both the rigid and the elastic cases and for three different sizes of the simulation domain. As shown by these curves, the spiraling rotation period [Fig. 3(a)] is not affected by a change of size of the simulation domain for both situations. In contrast, the unpinning bands [Figs. 3(b) and 3(c)] behave differently. In fact, whereas the electroelastic trend always seems to follow the same defibrillation points, the rigid case reduces the unpinning periods as the ratio between the obstacle radius and the domain size increases, specifically when $R_{ob}/L \geqslant 0.2$. This result is in agreement with the recent work of Cherry and Fenton [56] where no-flux boundary conditions effects have been criticized for purely electric physiological models.

In Fig. 4 we report a comprehensive sequence for defibrillation events, both rigid and elastic, for $R = 1.2$ cm and $L = 6$ cm with the same pacing period $T = 100$ ms. The figure enhances the mechanical effects on the unpinning dynamics in both shape propagating waves and timing. In fact, starting from the same initial conditions, the AP shape sequence is very similar, in accordance with the similar unpinning bands found,

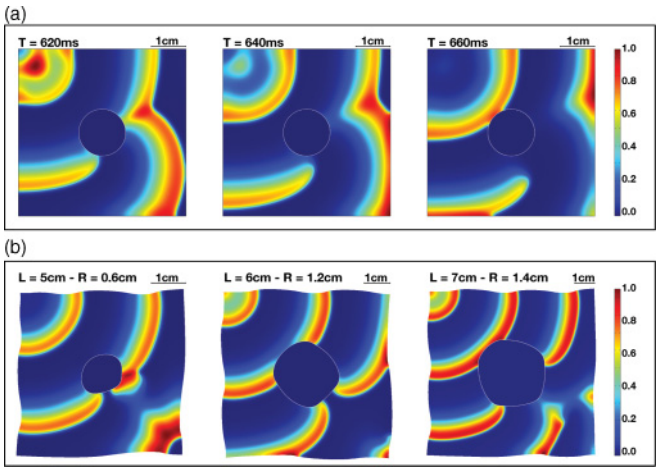

FIG. 5. (Color online) Differences induced by (a) pacing site and (b) elasticity. (a) Defibrillation sequence in the case of the pacing electrode inside the tissue (top left), confirming that the unpinning dynamics are similar to those observed with the pacing at the corner of the domain ($L = 5$ cm and $T = 98$ ms). (b) Three different domain sizes $L = 5,6,7$ cm with different obstacle sizes $R_{ob} = 0.6,1.2,1.4$ cm reporting an example of the distorted obstacle shapes varying in time due to the presence of elastic effects. The color map referred to is the normalized action potential of the Fenton-Karma model [38].

while the successful unpinning events occur for the elastic case before the rigid one, which is consistent with the separation of rotational periods shown before.

In Fig. 5 we show the differences induced by both pacing site and elasticity. A defibrillation sequence is reported in Fig. 5(a) for the case of the pacing electrode inside the tissue. The defibrillation dynamics is similar to the previous cases, reported in Fig. 4, suggesting that for the simplest scenario we modeled, differences in pacing sites seem to not affect the overall dynamics. In Fig. 5(b) three domains ($L = 5,6,7$ cm) with different obstacle sizes ($R_{ob} = 0.6,1.2,1.4$ cm) are reported to show the different shapes induced on the obstacle geometry by propagating AP waves. The obstacle gets distorted from a circle toward a sort of ellipse, evidencing the strong nonlinearity introduced by finite elasticity.

IV. DISCUSSION

The study carried out in this paper is relevant for the clinical necessity of obtaining the highest efficiency for low-energy implantable defibrillation devices [20]. The problem to identify, both theoretically and experimentally, is the correct periods of the electrical stimuli necessary to detach and remove the electrical reentries [17] (a procedure here denoted as the unpinning band search), which should possibly take into account the electromechanical properties of a real pulsing heart. Concretely, lower pacing rates would save the tissue from a further induction of arrhythmia and, by using a smaller amount of delivered energy, would also save the mean life of the implantable device itself.

Here we have initiated such an analysis. In a first approximation, we have specifically limited our numerical study to a simple mechanoelectric electrophysiological model, i.e., a two-dimensional heterogeneous, isotropic medium where a circular heterogeneity in the domain has been modeled as a nonexcitable area and capable of attaching action potential waves in a persistent manner (pinning), thus comparing the same stimulation protocol for both a purely electric (rigid) and electromechanic (elastic) model.

The associated feedback has been implemented by directly connecting the voltage conductivity tensor to the deformation and not taking into account other more biologically accurate feedback mechanisms such as stretch activated currents (see Refs. [39,40] and references therein for a discussion). The authors are well aware that this work has only touched the surface of an extremely complicated phenomenon. Even providing these simplifying assumptions, however, the presence of an active stress tensor, coming from a multiplicative decomposition procedure, has made the modeling nontrivial from both the theoretical and numerical points of view. Comparing the rigid and elastic models, in fact, we observed separating spiral rotational periods for increasing obstacle radii and similar unpinning band shapes. These results appear to be insensitive to the location of the pacing stimulus in both cases. We stress again that the mechanical coupling does not seem, for this specific situation studied at least, to play a major role in the pinning-unpinning dynamics. The nature of the equations involved in both the elastic and mechanical cases, however, does not mean that in other different scenarios, such as studies of free spiral dynamics on large domains, the role of the elastic coupling could be minor. We point out moreover that a more biologically accurate contractile heart model [50] could better reveal these differences in comparison with the nonelastic case. For this purpose it will be necessary to extend the proposed model to a NMR imported three-dimensional cardiac domain with tissue heterogeneity and fiber anisotropy, possibly revealing more complex dynamics, in analogy with already existing purely electrical studies (see Refs. [57,58] for an example).

The complex dynamic behavior of three-dimensional structures in excitable systems represents a current topic research in many related fields [59–63], where pinning, drifting, and detaching effects are being explored. This aspect thus plays a key role in further increasing the defibrillation efficiency mentioned, starting with simplified theoretical analysis [49,64–68].

The final goal in any case will be to increase the existing data on defibrillation efficiency even more by reducing the energy dispersion in the tissue by taking into account the complete phenomenology of the tissue. In this spirit, the evidence of a remarkable electromechanic role in pinning phenomena suggests the necessity of planning more advanced experiments to be performed in order to fine-tune the electrophysiological and biomechanical experimental data of the nonlinear cardiac tissue dynamics.

ACKNOWLEDGMENTS

Two of the authors (C.C. and S.F.) acknowledge the International Center for Relativistic Astropyhsics Network (ICRAnet) for partial support of this work.

[1] A. T. Winfree, *When Time Breaks Down: The Three-Dimensional Dynamics of Electrochemical Waves and Cardiac Arrhythmias* (Princeton University Press, Princeton, 1987).

[2] A. T. Winfree, *The Geometry of Biological Time*, 2nd ed. (Springer, Berlin, 2001).

[3] M. C. Cross and P. C. Hohenberg, Rev. Mod. Phys. **65**, 851 (1993).

[4] S. Sinha, A. Pande, and R. Pandit, Phys. Rev. Lett. **86**, 3678 (2001).

[5] S. Takagi, A. Pumir, D. Pazo, I. Efimov, V. Nikolski, and V. Krinsky, Phys. Rev. Lett. **93**, 058101 (2004).

[6] H. Zhang, Z. Cao, N. J. Wu, H. P. Ying, and G. Hu, Phys. Rev. Lett. **94**, 188301 (2005).

[7] G. Blatter, M. V. Feigel'man, V. B. Geshkenbein, A. I. Larkin, and V. M. Vinokur, Rev. Mod. Phys. **66**, 1125 (1994).

[8] J. M. Davidenko, A. V. Pertsov, R. Salomonsz, W. Baxter, and J. Jalife, Nature (London) **355**, 349 (1992).

[9] S. Alonso, F. Sagues, and A. S. Mikhailov, Science **299**, 1126 (2003).

[10] J. Keener and J. Sneyd, *Mathematical Physiology* (Springer, Berlin, 2001).

[11] V. Krinsky and K. Agladze, Physica D **8**, 50 (1983).

[12] K. Agladze, M. W. Kay, V. Krinsky, and N. Sarvazyan, Am. J. Physiol. Heart Circ. Physiol. **293**, H503 (2007).

[13] G. Gottwald, A. Pumir, and V. Krinsky, Chaos **11**, 487 (2001).

[14] V. I. Krinsky, V. N. Biktashev, and A. M. Pertsov, Ann. NY Acad. Sci. **591**, 232 (1990).

[15] L. Glass and M. E. Josephson, Phys. Rev. Lett. **75**, 2059 (1995).

[16] A. Pumir, V. Nikolski, M. Horning, A. Isomura, K. Agladze, K. Yoshikawa, R. Gilmour, E. Bodenschatz, and V. Krinsky, Phys. Rev. Lett. **99**, 208101 (2007).

[17] A. Pumir, S. Sinha, S. Sridhar, M. Argentina, M. Horning, S. Filippi, C. Cherubini, S. Luther, and V. Krinsky, Phys. Rev. E **81**, 010901(R) (2010).

[18] A. M. Pertsov, E. A. Ermakova, and A. V. Panfilov, Physica D **14**, 117 (1984).

[19] Z. Y. Lim, B. Maskara, F. Aguel, R. J. Emokpae, and l. Tung, Circulation **114**, 2113 (2006).

[20] S. Luther, F. H. Fenton, B. G. Kornreich, A. Squires, P. Bittihn, D. Hornung, M. Zabel, J. Flanders, A. Gladuli, L. Campoy, E. M. Cherry, G. Luther, G. Hasenfuss, V. I. Krinsky, A. Pumir, R. F. J. Gilmour, and E. Bodenschatz, Nature (London) **475**, 235 (2011).

[21] V. V. Fedorov, I. T. Lozinsky, E. A. Sosunov, E. P. Anyukhovsky, M. R. Rosen, C. W. Balke, and I. R. Efimov, Heart Rhythm **4**, 619e26 (2007).

[22] T. L. Riemer, E. A. Sobie, and L. Tung, Am. J. Physiol. Heart. Circ. Physiol. 44 **275**, H431 (1998).

[23] T. Heimburg and A. D. Jackson, Proc. Natl. Acad. Sci. USA **102**, 9790 (2005).

[24] D. Bini, C. Cherubini, and S. Filippi, Phys. Rev. E **72**, 041929 (2005).

[25] L. L. Demer and F. C. P. Yin, J. Physiol. **339**, 615 (1983).

[26] H. A. Spurgeon, M. D. Stern, G. Baartz, S. Raffaeli, R. G. Hansford, A. Talo, E. G. Lakatta, and M. C. Capogrossi, Am. J. Physiol. Heart Circ. Physiol. **258**, H574 (1990).

[27] M. S. Sacks and C. J. Chuong, J. Biomech. Eng. **115**, 202 (1993).

[28] G. C. J. Engelmayr, M. Cheng, C. J. Bettinger, J. T. Borenstein, R. Langer, and L. E. Freed, Nature Mater. **7**, 1003 (2008).

[29] S. Langeland, J. Dhooge, P. F. Wouters, H. A. Leather, P. Claus, B. Bijnens, and G. R. Sutherland, Circulation **112**, 2157 (2005).

[30] T. Edvardsen, B. L. Gerber, J. Garot, D. A. Bluemke, J. A. C. Lima, and O. A. Smiseth, Circulation **106**, 50 (2002).

[31] P. Kohl and F. Sachs, Philos. Trans. R. Soc. London Ser. B **359**, 1173 (2001).

[32] *Mechanosensitivity Ion Channels*, edited by A. Kamkin and I. Kiseleva (Springer, Dordrecht, 2010).

[33] R. Kaufmann and U. Theophile, Pflugers Arch. Gesamte Physiol. Menschen Tiere **297**, 174 (1967).

[34] P. Kohl, C. Bollensdorff, and A. Garny, Exp. Physiol. **91**, 307 (2006).

[35] P. Kohl and D. Noble, Prog. Biophys. Mol. Biol. **97**, 159 (2008).

[36] M. R. Franz, R. Cima, D. Wang, D. Profitt, and R. Kurz, Circulation **86**, 968 (1992).

[37] P. Nardinocchi and L. Teresi, J. Elast. **88**, 27 (2007).

[38] F. Fenton and A. Karma, Chaos **8**, 1054 (1998).

[39] C. Cherubini, S. Filippi, P. Nardinocchi, and L. Teresi, Prog. Biophys. Mol. Biol. **97**, 562 (2008).

[40] C. Cherubini, S. Filippi, P. Nardinocchi, and L. Teresi, in *Mechanosensitivity of the Heart: Mechanosensitivity in Cells and Tissues* , edited by A. Kamkin and I. Kiseleva (Springer, Berlin, 2009), Vol. 3, p. 12.

[41] P. J. Hunter, A. D. McCulloch, and H. E. D. J. ter Keurs, Prog. Biophys. Mol. Biol. **69**, 289 (1998).

[42] M. P. Nash and A. V. Panfilov, Prog. Biophys. Mol. Biol. **85**, 501 (2004).

[43] A. V. Panfilov, R. H. Keldermann, and M. P. Nash, Phys. Rev. Lett. **95**, 258104 (2005).

[44] A. V. Panfilov, R. H. Keldermann, and M. P. Nash, Proc. Natl. Acad. Sci. USA **104**, 7922 (2007); **104**, 20142(E) (2007).

[45] V. A. Lubarda, Appl. Mech. Rev. **57**, 95 (2004).

[46] A. L. M. Spencer, *Continuum Mechanics* (Dover, New York, 2004).

[47] G. A. Holzapfel, *Nonlinear Solid Mechanics: A Continuum Approach for Engineering* (Wiley, Chichester, 2000).

[48] M. P. Nash and P. Hunter, J. Elast. **61**, 113 (2000).

[49] P. Pelce, J. Sun, and C. Langeveld, Chaos Solitons Fractals **5**, 383 (1995).

[50] *Mathematically Modeling the Electrical Activity of the Heart: From Cell to Body Surface and Back Again*, edited by A. J. Pullan, M. L. Buist, and L. K. Cheng (World Scientific, Singapore, 2005).

[51] [http://www.pardiso-project.org/].

[52] F. E. Curtis, O. Schenk, and A. Wachter, SIAM J. Sci. Comput. **32**, 3447 (2010).

[53] [http://www.comsol.com].

[54] *Computational Cell Biology*, edited by C. Fall, E. Marland, J. Wagner, and J. Tyson (Springer, New York, 2002).

[55] R. J. Atkin and N. Fox, *An Introduction of the Theory of Elasticity* (Dover, New York, 2005).

[56] E. M. Cherry and F. H. Fenton, J. Theor. Biol. **285**, 164 (2011).

[57] A. V. Panfilov, Phys. Rev. E **59**, R6251 (1999).

[58] R. H. Keldermann, M. P. Nash, and A. V. Panfilov, Physica D **238**, 1000 (2009).

[59] Z. A. Jimenez, B. Marts, and O. Steinbock, Phys. Rev. Lett. **102**, 244101 (2009).

[60] Z. A. Jimenez and O. Steinbock, Europhys. Lett. **91**, 50002 (2010).

[61] S. Dutta and O. Steinbock, Phys. Rev. E **81**, 055202(R) (2010).

[62] S. Dutta and O. Steinbock, Phys. Rev. E **83**, 056213 (2011).

[63] S. Dutta and O. Steinbock, J. Phys. Chem. Lett. **2**, 945 (2011).

[64] R. R. Aliev and A. V. Panfilov, Chaos Solitons Fractals **7**, 293 (1996).

[65] V. N. Biktashev, A. V. Holden, M. A. Tsyganov, J. Brindley, and N. A. Hill, Phys. Rev. Lett. **81**, 2815 (1998).

[66] A. P. Munuzuri, C. Innocenti, J. M. Flesselles, J. M. Gilli, K. I. Agladze, and V. I. Krinsky, Phys. Rev. E **50**, R667 (1994).

[67] J. H. E. Cartwright, V. M. Eguiluz, E. H. Garcia, and O. Piro, Int. J. Bif. Chaos **9**, 2197 (1999).

[68] V. S. Zykov, G. Bordiougov, H. Brandtstadter, I. Gerdes, and H. Engel, Phys. Rev. Lett. **92**, 018304 (2004).